Journal of Alloys and Compounds 748 (2018) 411–417

Contents lists available at ScienceDirect

Journal of Alloys and Compounds

journal homepage: http://www.elsevier.com/locate/jalcom

Improving the ozone gas-sensing properties of $CuWO_4$ nanoparticles

Ariadne C. Catto [a, *], Tomas Fiorido [b], Érica L.S. Souza [c], Waldir Avansi Jr. [d], Juan Andres [e], Khalifa Aguir [b], Elson Longo [a], Laécio S. Cavalcante [c], Luís F. da Silva [d]

[a] Institute of Chemistry, São Paulo State University, P.O. Box 355, 14801–907, Araraquara, SP, Brazil
[b] Aix-Marseille University, CNRS IM2NP (UMR 7334), FS St Jérôme S152, Marseille, 13397, France
[c] PPGQ-CCN, Piauí State University, P.O. Box 381, 64002-150, Teresina, PI, Brazil
[d] Laboratory of Nanostructured Multifunctional Materials, Department of Physics, Federal University of São Carlos, 13565-905, São Carlos, SP, Brazil
[e] Department of Physics and Chemistry, Jaume I University, Castellón de la Plana, Spain

ARTICLE INFO

Article history:
Received 27 November 2017
Received in revised form
7 March 2018
Accepted 9 March 2018
Available online 13 March 2018

Keywords:
Sonochemical
$CuWO_4$
Surface
Chemiresistor
Ozone

ABSTRACT

This paper consists of an experimental investigation on the effects of annealing temperature on the structural, surface and ozone gas-sensing properties of $CuWO_4$ nanoparticles prepared via a sonochemical route. X-ray diffraction patterns and X-ray absorption near-edge structure spectroscopy revealed that both long- and short-order structures increase with the annealing temperature. Electrical resistance measurements indicated that $CuWO_4$ samples were sensitive in the range of 15–1400 ppb, exhibiting a good reversibility and repeatability. The enhancement of the ozone gas-sensing properties was attributed to the reduction of hydroxyl species and the improvement of the crystallization degree. This study provides a versatile strategy for obtaining $CuWO_4$ nanoparticles for practical applications as an ozone gas sensor.

1. Introduction

Nowadays, the development of gas sensors based on semiconductor metal oxides has been an effective way to obtain high-performance devices, which have been employed for environmental, industrial, agricultural, and automotive monitoring [1,2]. In this way, the manufacture of highly sensitive, selective, reliable and compact sensing devices to detect and measure gas concentrations provides a proper control and allow to monitor their emissions in the atmosphere [3–5].

Transition metal tungstates are a class of functional materials with remarkable properties [6–9]. Among the tungstates, much attention has been devoted to copper tungstate ($CuWO_4$) compounds because of their multifunctional properties, such as, photoluminescent, magnetic, and multiferroic properties [8,10,11]. In the past, the $CuWO_4$ compound has been applied mainly as a photoanode in electrochemical devices [8,9,12–14], and photocatalysts [15]. Few studies have been found regarding the gas-sensing properties of pristine $CuWO_4$ compounds. Gonzalez and co-workers investigated the nitric oxide (NO) sensing properties of $CuWO_4$ films deposited by pulsed laser deposition technique, which exhibited a high response towards NO gas, besides a stable and reproducible response [10].

It is known that both ozone (O_3) and carbon monoxide (CO) gases near the ground can cause risks to human health. Since O_3 gas is not emitted directly into the atmosphere, its production is directly related to gas pollutants including CO and NO_x, which in the presence of sunlight act as precursor sources to produce such gas. It is absorbed via respiratory tract, and consequently has been associated with asthma risks and changes in pulmonary function [16], while CO gas is hazardous to human health because of its combination with hemoglobin, reducing the oxygen delivery capacity of blood [17]. The World Health Organization (WHO) recommends a maximum daily 8-hour average of CO and O_3 concentrations of up to 8 ppm (parts per million) and 50 ppb (parts per billion), respectively.

Once few papers have reported the gas-sensing properties of pristine $CuWO_4$ compounds, their ozone gas-sensing properties have been rarely found. Therefore, a study of their gas sensor performance upon ozone exposure and the relationship between annealing temperature and $CuWO_4$ properties is required.

In this way, this manuscript addresses a facile approach for

* Corresponding author.
E-mail address: ade.catto@gmail.com (A.C. Catto).

https://doi.org/10.1016/j.jallcom.2018.03.104
0925-8388/

preparing sensing materials based on $CuWO_4$ nanoparticles via a sonochemical method. We investigated the influence of annealing temperature on structural and surface properties, correlating them with the ozone gas-sensing properties of the as-prepared $CuWO_4$ samples. Their properties were studied by X-ray diffraction (XRD), X-ray absorption near edge structure spectroscopy (XANES), X-ray photoelectron spectroscopy (XPS) and scanning electron microscopy (FE-SEM). Electrical measurements revealed that the ozone gas-sensing performance considerably improved as the annealing temperature increased. Furthermore, the $CuWO_4$ compound also detected sub-ppm ozone levels (ca. 15 ppb) and presented a low response to CO gas.

2. Experimental section

2.1. Synthesis procedure

As previously reported, nanostructured $CuWO_4$ powders were synthesized via a sonochemical method using sodium tungstate dihydrate ($Na_2WO_4{\cdot}2H_2O$; 99.5%) and copper nitrate trihydrate ($Cu(NO_3)_2{\cdot}3H_2O$; 99%) as reagents (Aldrich Company) [14,18]. The as-obtained amorphous powder was weighted and then divided into 3 equal portions. Afterwards, the powders were annealed in an electric oven under air atmosphere for 1 h at 300, 400, and 500 °C at a heating rate of 5 °C min^{-1}. The samples were identified according to their annealing temperature, i.e., CW300, CW400, and CW500, respectively.

2.2. Characterization techniques

The samples were characterized by X-ray diffraction (XRD) with a 0.02° step at a 2° min^{-1} scanning speed using CuKα radiation (Rigaku, DMax 2500 PC IV). The electronic and local atomic structures around tungsten (W) atoms were probed using X-ray near-edge absorption spectroscopy (XANES). The W-L_3 XANES spectra of the $CuWO_4$ samples were collected at the LNLS (Brazilian Laboratory of Synchrotron Radiation) facility employing the D04B-XAFS1 beamline. XANES data were collected at the W-L_3 in a transmission mode at room temperature using a Si(111) channel-cut monochromator. XANES spectra were recorded for each sample with energy steps of 1.0 eV before and after the edge, and 0.7 and 0.9 eV near the edge region for L_3 edge, respectively. The analyses of XAS spectra were performed using IFEFFIT package [19]. X-ray photoelectron spectroscopy (XPS) analyses were performed on a ScientaOmicron (model ESCA+) spectrometer using monochromatic AlKα (1486.6 eV) radiation. Peak decomposition was performed using a 70% Gaussian and 30% Lorentzian line shape with a Shirley nonlinear sigmoid-type baseline. The binding energies were corrected for charging effects by assigning a value of 284.8 eV to the adventitious C 1s line. The data were analyzed using CasaXPS software (Casa Software Ltd., U.K.). Morphological features of the samples were characterized using a scanning electron microscope with a field emission gun (FE-SEM, FEI INSPECT F50). The mean particle size was estimated from the analysis of SEM micrographs through the measure of approximately 100 nanoparticles.

2.3. Gas-sensing measurements

To perform gas-sensing measurements, the samples were prepared following the procedure adopted by our group [2,20,21]. $CuWO_4$ nanoparticles were dispersed in isopropyl alcohol by an ultrasonic cleaner for 30 min, and the suspension was then dripped onto a SiO_2/Si substrate with 120 nm thick Pt electrodes separated by a distance of 50 mm. The sensor samples were then annealed for 1 h at 300 °C. The details regarding the preparation of the electrodes and the system used for gas-sensing characterizations have already been published elsewhere [2,22–24].

The sensing properties of $CuWO_4$ nanoparticles towards ozone (O_3) and carbon monoxide (CO) gases were evaluated. The sensor operating temperature, which varied from 200 °C to 290 °C, was maintained by an external heating source based on an Hg lamp driven by a regulated power supply. Dry air was used both as a reference and the carrier gas, maintaining a constant total flow of 500 SCCM via mass flow controllers. Ozone gas was formed from oxidizing oxygen molecules of dry air by a calibrated pen-ray UV lamp (UVP, model P/N 90-0004-01), resulting in an O_3 output level from 15 to 1400 ppb. The ozone levels were calibrated by a toxic gas detector (ATI, model F12). The applied *dc* voltage was 1 V, and the electrical resistance was measured by an electrometer (HP4140B Source/Pico-ammeter). The CO gas sensing measurements were performed in the range of 30 and 90 ppm. It should be noted that 30 ppm was the lowest CO level available in our workbench.

The sensor response (S) is defined as $S = R_{gas}/R_{air}$ for O_3 gas, and $S = R_{air}/R_{gas}$ for CO gas, where R_{gas} and R_{air} are the electric resistance of the sensor sample exposed to the target gas and air, respectively. The sensor response time was defined as the time required for the electrical resistance to reach 90% of the initial value when exposed to the investigated gas. Similarly, the recovery time was defined as the time required for the electrical resistance to recover 90% of the initial value after switching off the target gas flow.

3. Results and discussion

3.1. Long- and short-range structure analysis

XRD patterns of the CW300, CW400 and CW500 samples are displayed in Fig. 1(a–c), respectively.

As it can be observed in Fig. 1(a,b), XRD patterns of the CW300 and CW400 samples present a mixture of $CuWO_4{\cdot}2H_2O$ and $CuWO_4$ phases. The annealing temperature at 400 °C eliminates the water molecules present in the $CuWO_4{\cdot}2H_2O$ phase. In a previous study [18], we described the $CuWO_4{\cdot}2H_2O$ as a crystalline phase presenting a monoclinic structure, in accordance with the Joint Committee on Powder Diffraction Standards (JCPDS) file 33-0503. Furthermore, XRD patterns indicate that a long-range order

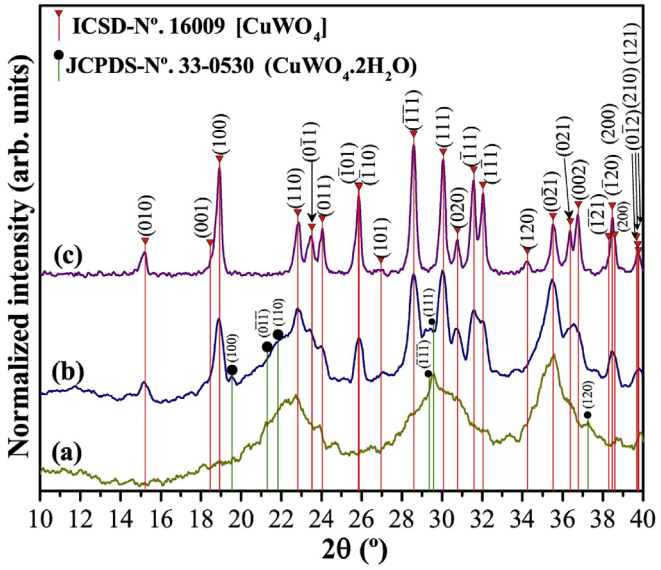

Fig. 1. XRD patterns of $CuWO_4$ samples annealed during 1 h at different temperatures: (a) CW300, (b) CW400, and (c) CW500.

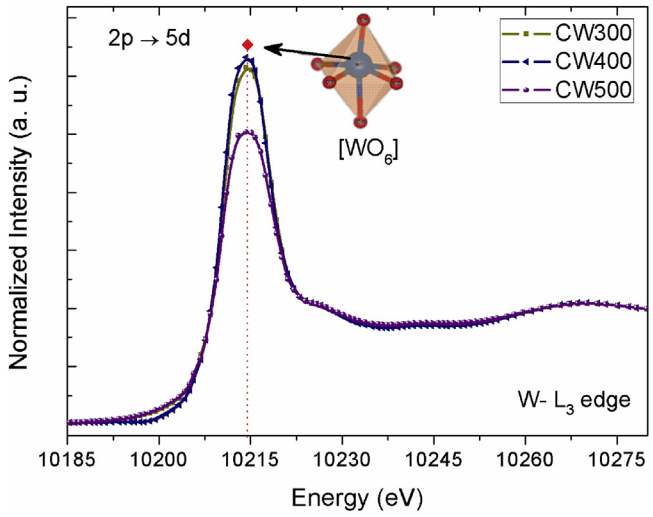

Fig. 2. XANES spectra in the W-L_3 edge for $CuWO_4$ samples annealed during 1 h at different temperatures: (a) CW300, (b) CW400, and (c) CW500.

structure is entirely obtained at 500 °C, as seen in Fig. 1(c). All the reflections (CW500 sample) were indexed to a pristine $CuWO_4$ triclinic structure, according to the Inorganic Crystal Structure Database (ICSD) file 16009.

In the last years, our group has been employing the XANES spectroscopy to study the local order and electronic structure in different materials which present order-disorder characteristics related to the synthetic approach [22,23,25–27]. Thus, such technique was employed to analyze the effect of the annealing treatment on the studied samples. Fig. 2 shows the W L_3-edge of $CuWO_4$ samples annealed at different temperatures.

According to previous reports, the W L-edge XANES spectrum provides information on the electronic state and the geometry of the tungsten species [6,28–30]. Considering the XANES spectra in the W L_3-edge, the as-synthesized samples present a pronounced difference related to the white line of the XANES spectrum, which can be attributed to electron transitions from a 2*p* 3/2 state to a vacant 5d state, showing that the form and shape of the white line is sensitive to the structure [28]. According to the qualitative analyses of XRD patterns and W L_3-edge XANES spectra of $CuWO_4$ samples, the difference observed on the white line absorption edge (W L_3) among $CuWO_4$ samples as a function of the annealing temperature could be related to the enhancement of structural ordering at short and medium range, as well as a major bond strength between the (O→W→O), which promotes an improvement of periodicity in distorted octahedral [WO_6] clusters, as seen in the inset of Fig. 2.

3.2. Surface analysis

XPS analyses were performed to probe detailed information on the surface properties of the CW300 and CW500 samples. In the high-resolution Cu $2p_{3/2}$ XPS spectra shown in Fig. 3a, a peak was observed at approximately 934.9 eV and two satellite peaks, which are consistent with the Cu^{2+} oxidation state [31,32]. Additionally, the binding energy of Cu $2p_{3/2}$ is close to the standard value for $Cu(OH)_2$, suggesting the presence of hydroxyl species [33,34]. Fig. 3(b) displays the high-resolution W 4f XPS spectra, in which the W $4f_{7/2}$ and W $4f_{5/2}$ peaks are centered at 35.4 eV and 37.5 eV, which is characteristic of W^{6+} ion [35,36]. The results indicate that the increase of the annealing temperature did not affect the oxidation state of metallic ions.

The high-resolution O 1 s region shown in Fig. 3(c) was decomposed into two components, labeled as O $1s_{(1)}$ and O $1s_{(2)}$. The lowest energy peak, O $1s_{(1)}$, at approximately 530.5 eV correspond to O^{2-} ions bound to Cu^{2+} and W^{6+} ions, while the O $1s_{(2)}$ peak at around 532.2 eV was attributed to hydroxyl groups or anion OH^- adsorbed on the materials surface. As it can be observed in Fig. 3(c), the surface hydroxyl species percentage reduces drastically from 92% to 7% as the annealing temperature increases. The OH^- species are desorbed by heating to temperatures higher than 400 °C [37].

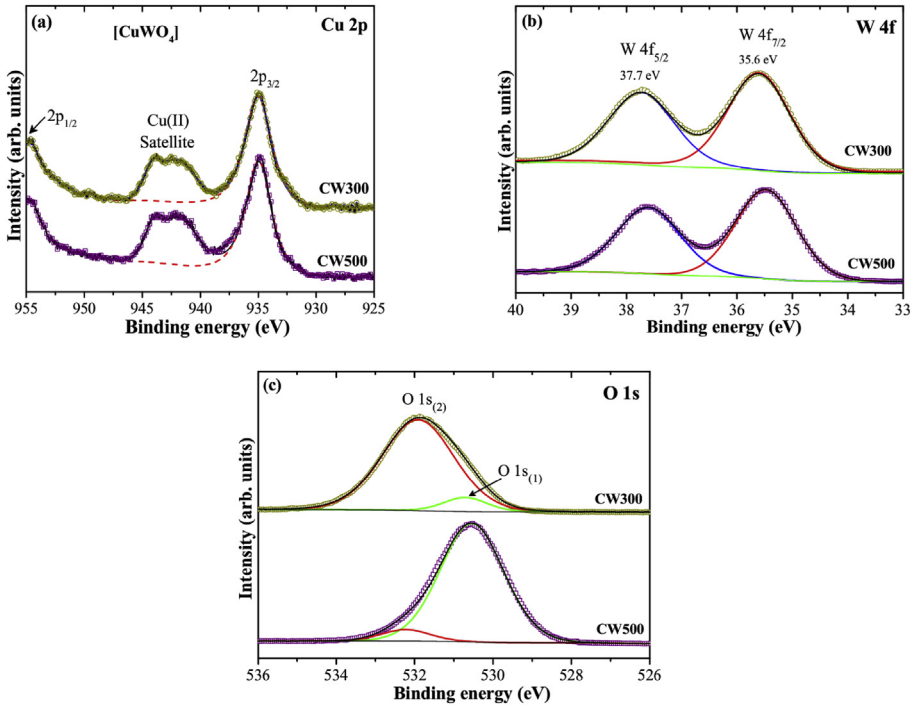

Fig. 3. XPS spectra of CW300 and CW500 samples. (a) Cu 2p, (b) W 4f, and (c) O 1s.

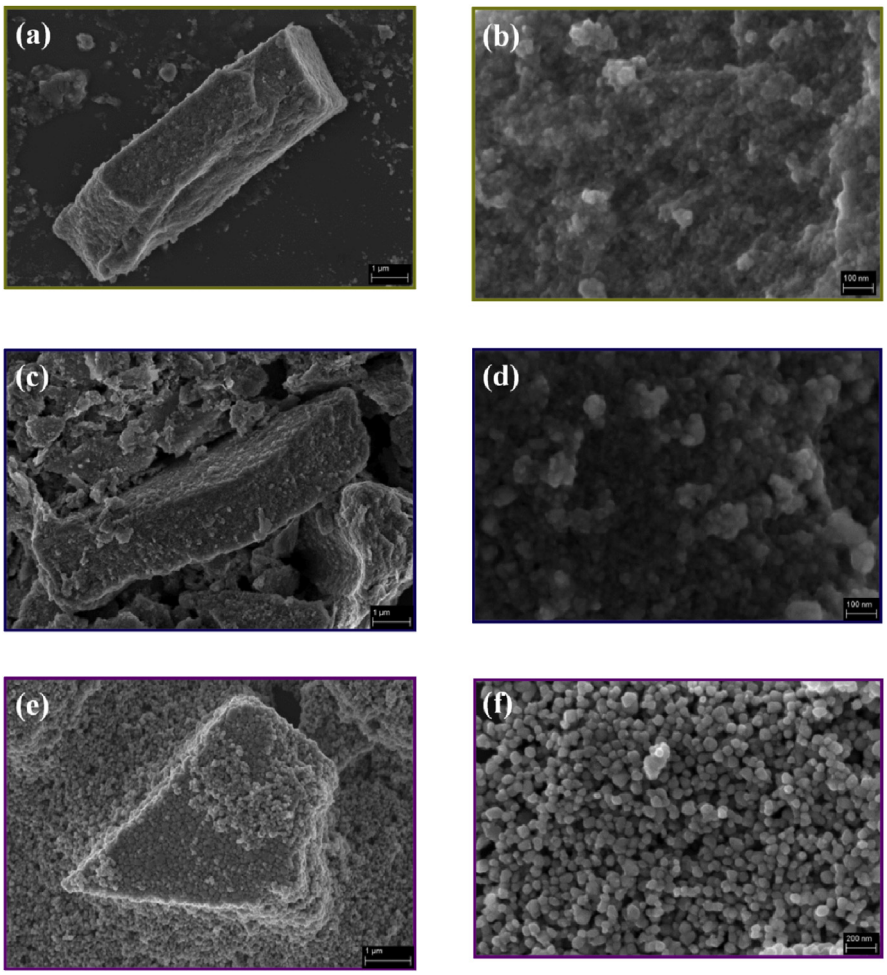

Fig. 4. FE-SEM images at low- and high-magnification of $CuWO_4$ samples annealed during 1 h at different temperatures: (a,b) CW300, (c,d) CW400, and (e,f) CW500.

3.3. Microstructural analysis

The FE-SEM micrographs of the CW300, CW400 and CW500 samples after annealing treatments are presented in Fig. 4 (a–f). They show strongly agglomerated nonuniform particles with neck formation and coalescence between the nanoparticles. We observed that the particle shape became well-defined and homogeneous as the annealing temperature increased, and that there was a gradual increase of the particle size from 15 to 66 nm. These results corroborate the classical growth model, since higher

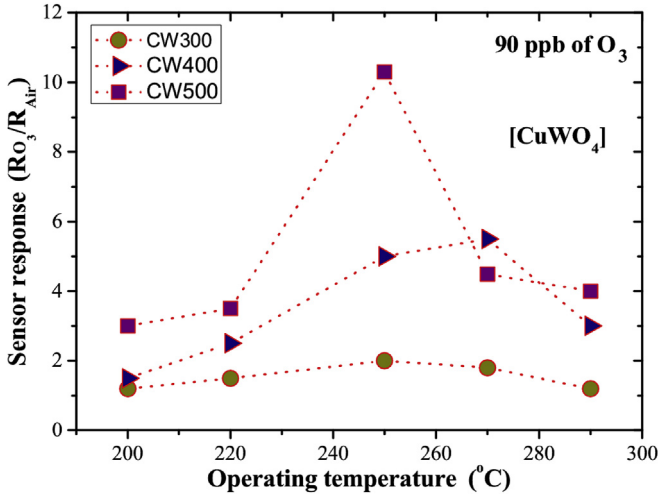

Fig. 5. Gas sensor response of $CuWO_4$ samples exposed to 90 ppb of O_3 at different operating temperatures.

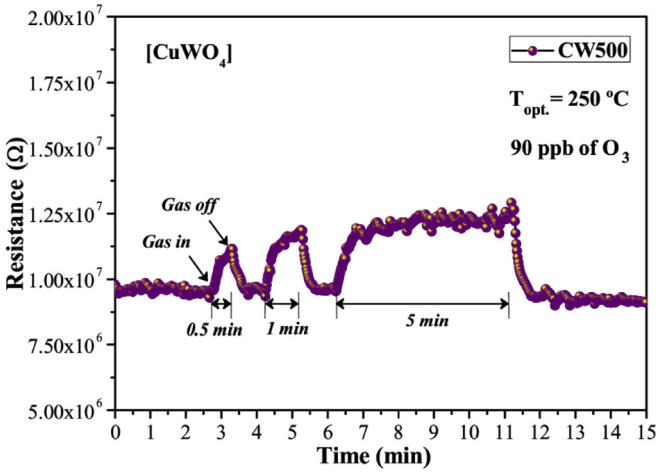

Fig. 6. Gas sensor response of the CW500 sample at 250 °C exposed to 90 ppb of O_3 gas for different exposure times.

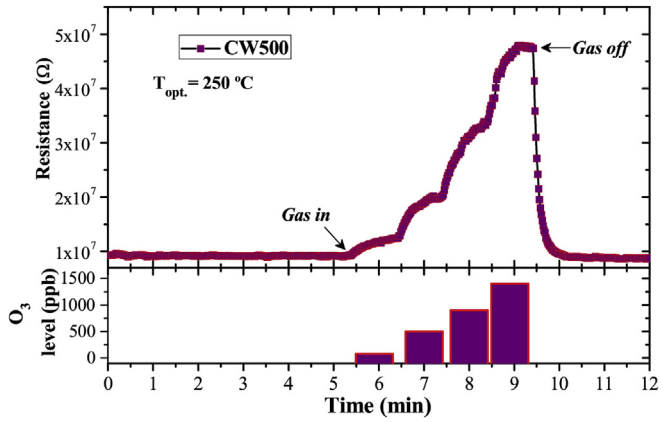

Fig. 7. Gas sensor response of the CW500 sample at an operating temperature of 250 °C exposed to different O_3 levels (80, 500, 900, and 1400 ppb).

annealing temperatures provide a large amount of energy, consequently favoring the particle growth as a result of reduced surface energy [38].

3.4. Gas-sensing properties

The gas-sensing performance of $CuWO_4$ nanoparticles was evaluated towards O_3 and CO gases. Initially, the best operating temperature of the samples was evaluated by exposing them during 1 min to 90 ppb of O_3 at different operating temperatures, as shown in Fig. 5. We observed that, for the CW400 and CW500 samples, the highest sensor response was obtained at around 270 and 250 °C, respectively, while for the CW300 sample, the response remained almost unchanged regardless of the operating temperature, as seen in Fig. 5. The sensor response values of $CuWO_4$ samples followed the order: CW500 > CW400 > CW300.

According to the literature, the sensor performance is strongly influenced by the presence of pre-adsorbed species on the semiconductor surfaces, crystallization degree, among others [22,37,39–44]. Katoch and co-workers reported that the annealing of ZnO nanofibers at high temperatures enhance their capability for gas detection [40]. The authors explained that the high crystallinity of ZnO reduces the number of carriers, improving the adsorption/desorption processes, and then enhancing the sensor response [40]. Regarding the surface hydroxylation of the sensing material, the presence of OH^- species hinders the adsorption of O_3 molecules onto sensing materials. Similar results were found by Steinhauer and co-workers, which verified that hydroxyl species reduce the active sites on the CuO surface, thus impairing the sensor response [44].

Therefore, it is reasonable to propose that the improvement in O_3 gas-sensing performance can be linked to the reduction of OH^- groups and the enhancement of structural properties of $CuWO_4$ nanoparticles as the annealing temperature increases.

Following, the CW500 sample was kept at 250 °C, and then exposed to 90 ppb of O_3 during different time intervals (0.5, 1.0, and 5.0 min). As it can be seen in Fig. 6, the electrical resistance is increased during an exposure to O_3 gas, a typical behavior of an n-type semiconductor [23]. This behavior can be explained by the adsorption of O_3 molecules on the $CuWO_4$ surface, where O^- anions extract electrons from the $CuWO_4$ compound. The gas sensing of $CuWO_4$ materials upon exposure to O_3 molecules can be explained by the following reactions [4,23]:

$$O_{2(ads)} + 2e^- \rightarrow 2O^-_{(ads)} \quad (1)$$

$$O_{3(gas)} + e^- \rightarrow O^-_{3\ (ads)} \quad (2)$$

$$O^-_{3\ (ads)} + O^-_{(ads)} + 2e^- \rightarrow O_{2\ (gas)} + 2O^-_{2\ (ads)} \quad (3)$$

Their depletion layer becomes thicker as the carrier concentration decreases, consequently increasing their electrical resistance [4,23].

Furthermore, we can observe that the CW500 sample rapidly detected the presence of O_3 molecules, even for a shorter exposure time (0.5 min). The average response time was approximately 7 s for all cases, while the recovery time varied from 5 to 10 s, depending on the exposure time. It is interesting to note that despite presenting a rapid detection, the sample saturation level was reached at exposure times longer than 0.5 min, as illustrated in Fig. 6.

The CW500 sample was kept at 250 °C, and then continuously exposed to different O_3 levels (80–1400 ppb), with each cycle lasting 1 min. Fig. 7 displays a gradual and greater sensor response as O_3 level increases, showing no evidence of sensor saturation. It should be noted that although the CW500 sample had been exposed to different ozone levels, these consecutive expositions did not poison the sample surface, as indicated by the total reversibility of the sample baseline after the interruption of O_3 gas flux. The recovery time after the consecutive expositions was approximately 30 s, revealing a rapid reversibility.

Further gas-sensing measurements were performed to investigate the detection limit of the CW500 sample in relation to O_3, as well as its sensitivity towards a reducing gas (here, CO). These experiments were carried out using an operating temperature of

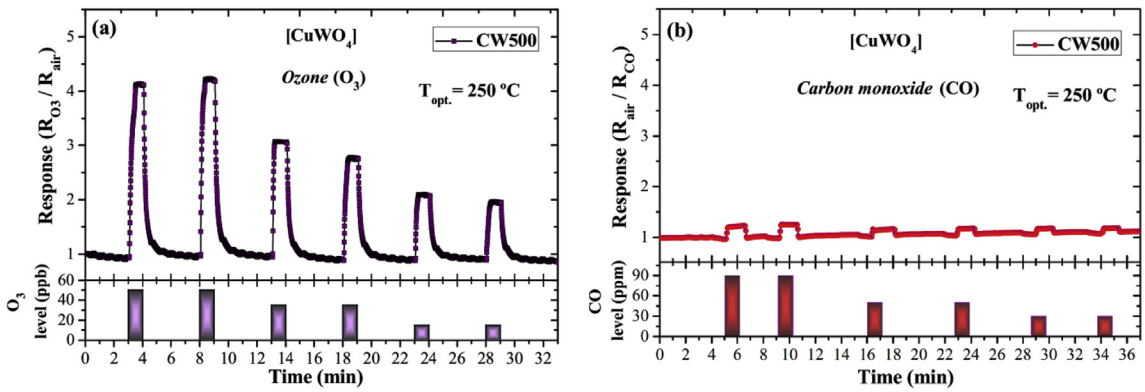

Fig. 8. Sensor response of the CW500 sample at 250 °C exposed to **(a)** 50, 35, and 15 ppb of O_3 gas and **(b)** 90, 50, and 30 ppm of CO gas.

250 °C and an exposure time of 1 min.

First, the CW500 sample was exposed to lower O_3 levels (15–50 ppb), as shown in Fig. 8(a). We can observe that the sample was sensitive to all O_3 levels investigated, exhibiting a good response as well as repeatability and reversibility characteristics. We should note here that O_3 is a harmful gas for human health, whose exposition to levels above 100 ppb is highly not recommended [2].

Afterwards, the CW500 sample was exposed to different concentrations of CO gas (30–90 ppm). For a good comparison between sensor responses, we chose to keep an identical Y-axis from Fig. 8(a,b). As depicted in Fig. 8(b), the sample also detected all the CO gas concentrations investigated, however, the sensor response presented was too low ($S = 1.2$), even for the highest CO gas level (90 ppm).

In order to investigate the selectivity, we compared the sensor response values of the CW500 sample when exposed to 1.4 ppm (or 1400 ppb) of O_3 (Fig. 7) and 30 ppm of CO (Fig. 8(b)). It was found that the response value to O_3 gas was approximately 5 times greater than to CO gas. These findings suggest that the CW500 sample can be considered a promising material for the development of ozone gas sensors for environmental applications.

4. Conclusions

In summary, $CuWO_4$ nanoparticles were obtained in this work via a sonochemical route, and then investigated as ozone gas sensor. XRD and XANES analyses indicated an increase of the (long- and short-range) crystallization degree as a function of the annealing temperature. The gas-sensing experiments revealed the enhancement of ozone-sensing properties for higher annealing temperatures. The sample annealed at 500 °C exhibited a low O_3 detection limit around 15 ppb, total recovery, and a low response to CO gas. The improved sensor performance can be associated with the reduction of hydroxyl groups and the enhancement of structural properties also as a function of the annealing temperature. These findings show that $CuWO_4$ nanoparticles exhibit remarkable properties for practical applications.

Acknowledgments

The authors would like to thank Prof. Valmor R. Mastelaro for XPS measurements. This work was supported by the following Brazilian research financing institutions: FAPESP (Proc. No. 2013/07296-2, 2017/10313-7 and 2017/12437-5) FAPEPI, CNPq (310863/2014-7 and 434266/2016-7), and CAPES. The research was partially performed at the Brazilian Nanotechnology National Laboratory (Microfabrication team; Project LMF-18580), and the Brazilian Laboratory of Synchrotron Radiation (LNLS, Project D04B-XAFS1-11883), both in Campinas, SP, Brazil. The author Juan Andrés acknowledges the financial support of the agencies: Generalitat Valenciana, Ministerio de Economia y Competitividad, and Programa de Cooperación Cientifica con Iberoamerica (Brazil), Ministerio de Educacion.

References

[1] D.R. Miller, S.A. Akbar, P.A. Morris, Nanoscale metal oxide-based heterojunctions for gas sensing: a review, Sens. Actuators B Chem. 204 (2014) 250–272. https://doi.org/10.1016/j.snb.2014.07.074.

[2] L.F. da Silva, A.C. Catto, W. Avansi, L.S. Cavalcante, J. Andres, K. Aguir, V.R. Mastelaro, E. Longo, A novel ozone gas sensor based on one-dimensional (1D) α-Ag_2WO_4 nanostructures, Nanoscale 6 (2014) 4058–4062, https://doi.org/10.1039/C3NR05837A.

[3] N. Joshi, L.F. da Silva, H.S. Jadhav, F.M. Shimizu, P.H. Suman, J.-C. M'Peko, M.O. Orlandi, J.G. Seo, V.R. Mastelaro, O.N. Oliveira Jr., Yolk-shelled $ZnCo_2O_4$ microspheres: surface properties and gas sensing application, Sens. Actuators B Chem. 257 (2018) 906–915. https://doi.org/10.1016/j.snb.2017.11.041.

[4] D. Barreca, D. Bekermann, E. Comini, A. Devi, R.A. Fischer, A. Gasparotto, C. Maccato, C. Sada, G. Sberveglieri, E. Tondello, Urchin-like ZnO nanorod arrays for gas sensing applications, CrystEngComm 12 (2010) 3419–3421, https://doi.org/10.1039/C0CE00139B.

[5] H.-J. Kim, J.-H. Lee, Highly sensitive and selective gas sensors using p-type oxide semiconductors: Overview, Sens. Actuators B Chem. 192 (2014) 607–627. https://doi.org/10.1016/j.snb.2013.11.005.

[6] S.M. AlShehri, J. Ahmed, T. Ahamad, P. Arunachalam, T. Ahmad, A. Khan, Bifunctional electro-catalytic performances of $CoWO_4$ nanocubes for water redox reactions (OER/ORR), RSC Adv. 7 (2017) 45615–45623, https://doi.org/10.1039/C7RA07256B.

[7] S.M. AlShehri, J. Ahmed, T. Ahamad, B.M. Almaswari, A. Khan, Efficient photodegradation of methylthioninium chloridedye in aqueous using barium tungstate nanoparticles, J. Nanoparticle Res. 19 (2017) 1–14, https://doi.org/10.1007/s11051-017-3970-z.

[8] M. Valenti, D. Dolat, G. Biskos, A. Schmidt-Ott, W.A. Smith, Enhancement of the photoelectrochemical performance of $CuWO_4$ thin films for solar water splitting by plasmonic nanoparticle functionalization, J. Phys. Chem. C 119 (2015) 2096–2104, https://doi.org/10.1021/jp506349t.

[9] C.R. Lhermitte, B.M. Bartlett, Advancing the chemistry of $CuWO_4$ for photoelectrochemical water oxidation, Acc. Chem. Res. 49 (2016) 1121–1129, https://doi.org/10.1021/acs.accounts.6b00045.

[10] C.M. Gonzalez, X. Du, J.L. Dunford, M.L. Post, Copper tungstate thin-films for nitric oxide sensing, Sens. Actuators B Chem. 173 (2012) 169–176. https://doi.org/10.1016/j.snb.2012.06.067.

[11] M. V Lalić, Z.S. Popović, F.R. Vukajlović, Ab initio study of electronic, magnetic and optical properties of $CuWO_4$ tungstate, Comput. Mater. Sci. 50 (2011) 1179–1186. https://doi.org/10.1016/j.commatsci.2010.11.018.

[12] J.E. Yourey, K.J. Pyper, J.B. Kurtz, B.M. Bartlett, Chemical stability of $CuWO_4$ for photoelectrochemical water oxidation, J. Phys. Chem. C 117 (2013) 8708–8718, https://doi.org/10.1021/jp402048b.

[13] N. Gaillard, Y. Chang, A. DeAngelis, S. Higgins, A. Braun, A nanocomposite photoelectrode made of 2.2 eV band gap copper tungstate ($CuWO_4$) and multi-wall carbon nanotubes for solar-assisted water splitting, Int. J. Hydrogen Energy 38 (2013) 3166–3176. https://doi.org/10.1016/j.ijhydene.2012.12.104.

[14] A.E.B. Lima, M.J.S. Costa, R.S. Santos, N.C. Batista, L.S. Cavalcante, E. Longo, G.E. Luz, Facile preparation of $CuWO_4$ porous films and their photoelectrochemical properties, Electrochim. Acta 256 (2017) 139–145. https://doi.org/10.1016/j.electacta.2017.10.010.

[15] Z. Barzgari, S.Z. Askari, A. Ghazizadeh, Fabrication of nanostructured $CuWO_4$ for photocatalytic degradation of organic pollutants in aqueous solution, J. Mater. Sci. Mater. Electron. 28 (2017) 3293–3298, https://doi.org/10.1007/s10854-016-5922-2.

[16] I.A. Yang, O. Holz, R.A. Jörres, H. Magnussen, S.J. Barton, S. Rodríguez, J.A. Cakebread, J.W. Holloway, S.T. Holgate, Association of tumor necrosis factor-α polymorphisms and ozone-induced change in lung function, Am. J. Respir. Crit. Care Med. 171 (2005) 171–176, https://doi.org/10.1164/rccm.200402-194OC.

[17] S. Ghosh, M. Narjinary, A. Sen, R. Bandyopadhyay, S. Roy, Fast detection of low concentration carbon monoxide using calcium-loaded tin oxide sensors, Sens. Actuators B Chem. 203 (2014) 490–496. https://doi.org/10.1016/j.snb.2014.06.111.

[18] E.L.S. Souza, J.C. Sczancoski, I.C. Nogueira, M.A.P. Almeida, M.O. Orlandi, M.S. Li, R.A.S. Luz, M.G.R. Filho, E. Longo, L.S. Cavalcante, Structural evolution, growth mechanism and photoluminescence properties of $CuWO_4$ nanocrystals, Ultrason. Sonochem. 38 (2017) 256–270. https://doi.org/10.1016/j.ultsonch.2017.03.007.

[19] B. Ravel, M. Newville, ATHENA, ARTEMIS, HEPHAESTUS: data analysis for X-ray absorption spectroscopy using IFEFFIT, J. Synchrotron Radiat. 12 (2005) 537–541, https://doi.org/10.1107/S0909049505012719.

[20] A.C. Catto, L.F. da Silva, M.I.B. Bernardi, M.S. Li, E. Longo, P.N. Lisboa-Filho, O.R. Nascimento, V.R. Mastelaro, An investigation into the influence of zinc precursor on the microstructural, photoluminescence, and gas-sensing properties of ZnO nanoparticles, J. Nanoparticle Res. 16 (2014) 1–9, https://doi.org/10.1007/s11051-014-2760-0.

[21] L.F. da Silva, J.-C. M'Peko, A.C. Catto, S. Bernardini, V.R. Mastelaro, K. Aguir, C. Ribeiro, E. Longo, UV-enhanced ozone gas sensing response of ZnO-SnO_2 heterojunctions at room temperature, Sens. Actuators B Chem. 240 (2017) 573–579. https://doi.org/10.1016/j.snb.2016.08.158.

[22] L.F. da Silva, V.R. Mastelaro, A.C. Catto, C.A. Escanhoela Jr., S. Bernardini, S.C. Zílio, E. Longo, K. Aguir, Ozone and nitrogen dioxide gas sensor based on a nanostructured $SrTi_{0.85}Fe_{0.15}O_3$ thin film, J. Alloys Compd. 638 (2015) 374–379. https://doi.org/10.1016/j.jallcom.2015.03.089.

[23] A.C. Catto, L.F. da Silva, M.I.B. Bernardi, S. Bernardini, K. Aguir, E. Longo, V.R. Mastelaro, Local structure and surface properties of $Co_xZn_{1-x}O$ thin films for ozone gas sensing, ACS Appl. Mater. Interfaces 8 (2016) 26066–26072, https://doi.org/10.1021/acsami.6b08589.

[24] L.F. da Silva, A.C. Catto, W. Avansi Jr., L.S. Cavalcante, V.R. Mastelaro, J. Andrés, K. Aguir, E. Longo, Acetone gas sensor based on α-Ag_2WO_4 nanorods obtained via a microwave-assisted hydrothermal route, J. Alloys Compd. 683 (2016) 186–190. https://doi.org/10.1016/j.jallcom.2016.05.078.

[25] L.F. da Silva, W. Avansi, J. Andres, C. Ribeiro, M.L. Moreira, E. Longo, V.R. Mastelaro, Long-range and short-range structures of cube-like shape

$SrTiO_3$ powders: microwave-assisted hydrothermal synthesis and photocatalytic activity, Phys. Chem. Chem. Phys. 15 (2013) 12386–12393, https://doi.org/10.1039/C3CP50643F.
[26] L.F. da Silva, J.-C. M'Peko, J. Andrés, A. Beltrán, L. Gracia, M.I.B. Bernardi, A. Mesquita, E. Antonelli, M.L. Moreira, V.R. Mastelaro, Insight into the effects of Fe addition on the local structure and electronic properties of $SrTiO_3$, J. Phys. Chem. C 118 (2014) 4930–4940, https://doi.org/10.1021/jp408839q.
[27] W. Avansi, L.J.Q. Maia, C. Ribeiro, E.R. Leite, V.R. Mastelaro, Local structure study of vanadium pentoxide 1D-nanostructures, J. Nanoparticle Res. 13 (2011) 4937, https://doi.org/10.1007/s11051-011-0472-2.
[28] S. Yamazoe, Y. Hitomi, T. Shishido, T. Tanaka, XAFS study of tungsten L1- and L3-edges: structural analysis of WO3 species loaded on TiO_2 as a catalyst for photo-oxidation of NH3, J. Phys. Chem. C 112 (2008) 6869–6879, https://doi.org/10.1021/jp711250f.
[29] G. Poirier, F.C. Cassanjes, Y. Messaddeq, S.J.L. Ribeiro, A. Michalowicz, M. Poulain, Local order around tungsten atoms in tungstate fluorophosphate glasses by X-ray absorption spectroscopy, J. Non Cryst. Solids 351 (2005) 3644–3648. https://doi.org/10.1016/j.jnoncrysol.2005.08.038.
[30] Y. Kou, B. Zhang, J. Niu, S. Li, H. Wang, T. Tanaka, S. Yoshida, Amorphous features of working catalysts: XAFS and XPS characterization of $Mn/Na_2WO_4/SiO_2$ as used for the oxidative coupling of methane, J. Catal. 173 (1998) 399–408. https://doi.org/10.1006/jcat.1997.1900.
[31] R.P. Vasquez, CuO by XPS, Surf. Sci. Spectra 5 (1998) 262–266, https://doi.org/10.1116/1.1247882.
[32] S. Poulston, P.M. Parlett, P. Stone, M. Bowker, Surface oxidation and reduction of CuO and Cu_2O studied using XPS and XAES, Surf. Interface Anal. 24 (1996) 811–820.
[33] R.P. Vasquez, $Cu(OH)_2$ by XPS, Surf. Sci. Spectra 5 (1998) 267–272, https://doi.org/10.1116/1.1247883.
[34] O. Akhavan, R. Azimirad, S. Safa, E. Hasani, $CuO/Cu(OH)_2$ hierarchical nanostructures as bactericidal photocatalysts, J. Mater. Chem. 21 (2011) 9634–9640, https://doi.org/10.1039/C0JM04364H.
[35] Z. Wen, W. Wu, Z. Liu, H. Zhang, J. Li, J. Chen, Ultrahigh-efficiency photocatalysts based on mesoporous Pt-WO_3 nanohybrids, Phys. Chem. Chem. Phys. 15 (2013) 6773–6778, https://doi.org/10.1039/C3CP50647A.
[36] S. Wang, S.V. Kershaw, G. Li, M.K.H. Leung, The self-assembly synthesis of tungsten oxide quantum dots with enhanced optical properties, J. Mater. Chem. C 3 (2015) 3280–3285, https://doi.org/10.1039/C5TC00278H.
[37] C. Wang, L. Yin, L. Zhang, D. Xiang, R. Gao, Metal oxide gas sensors: sensitivity and influencing factors, Sensors 10 (2010) 2088–2106, https://doi.org/10.3390/s100302088.
[38] C. Greskovich, K.W. Lay, Grain growth in very porous Al_2O_3 compacts, J. Am. Ceram. Soc. 55 (1972) 142–146, https://doi.org/10.1111/j.1151-2916.1972.tb11238.x.
[39] N. Barsan, D. Koziej, U. Weimar, Metal oxide-based gas sensor research: how to? Sens. Actuators B Chem. 121 (2007) 18–35. https://doi.org/10.1016/j.snb.2006.09.047.
[40] A. Katoch, G.-J. Sun, S.-W. Choi, J.-H. Byun, S.S. Kim, Competitive influence of grain size and crystallinity on gas sensing performances of ZnO nanofibers, Sens. Actuators B Chem. 185 (2013) 411–416. https://doi.org/10.1016/j.snb.2013.05.030.
[41] Z.M. Seeley, A. Bandyopadhyay, S. Bose, Influence of crystallinity on CO gas sensing for TiO_2 films, Mater. Sci. Eng. B 164 (2009) 38–43. https://doi.org/10.1016/j.mseb.2009.06.009.
[42] G. Korotcenkov, Metal oxides for solid-state gas sensors: what determines our choice? Mater. Sci. Eng. B 139 (2007) 1–23. https://doi.org/10.1016/j.mseb.2007.01.044.
[43] E.D. Skouras, V.N. Burganos, A.C. Payatakes, Simulation of gas diffusion and sorption in nanoceramic semiconductors, J. Chem. Phys. 110 (1999) 9244–9253, https://doi.org/10.1063/1.478848.
[44] S. Steinhauer, A. Chapelle, P. Menini, M. Sowwan, Local CuO nanowire growth on microhotplates: in situ electrical measurements and gas sensing application, ACS Sens. 1 (2016) 503–507, https://doi.org/10.1021/acssensors.6b00042.